# Comparative study of three methods for the simulation of two-dimensional photonic crystals

**Davy Pissoort, Bart Denecker, Peter Bienstman, Frank Olyslager, and Daniël De Zutter**

*Department of Information Technology, Ghent University, St.-Pietersnieuwstraat 41, Ghent, Belgium*

Three methods for the efficient simulation of two-dimensional photonic crystal structures are compared, namely, a semianalytical multiple-scattering technique; a vectorial eigenmode expansion technique; and a FDTD-ROM technique. The basic principles of each method are presented. For the semianalytical technique and for the vectorial eigenmode expansion technique, we show how reflections coming from abruptly terminated waveguides can be avoided. The main advantages and disadvantages of each method are discussed. Results from use of the three methods are compared for several photonic crystal structures. © 2004 Optical Society of America

*OCIS codes:* 000.4430, 260.1180, 230.7370.

## 1. INTRODUCTION

Photonic crystals (PCs) have aroused substantial interest because of their ability to control lightwave propagation.[1] Two-dimensional PCs consist of a set of parallel cylinders embedded in a homogeneous medium or a planar stratified medium. Because of the periodicity, a PC exhibits photonic bandgaps in which electromagnetic fields cannot propagate in given directions. By creating different types of defects in a PC, it is possible to create waveguides with sharp bends,[2–4] lasers,[5] multiplexers,[6–8] etc.

To design and simulate PC circuits efficiently, many different numerical techniques have been proposed. Probably the most popular technique is the finite-difference time-domain technique (FDTD) owing to the simplicity of the algorithm and the flexibility regarding the structure and the materials. By means of this time-domain method, one can obtain information over a wide frequency range by performing a single simulation followed by a Fourier transform. However, as PCs consist of objects that are rather small compared with the wavelength, a small space step is required for a correct discretization. As a consequence, computer memory requirements rise excessively if the standard FDTD method is used. The smaller time step that needs to be used also leads to excessive computing time. One way to overcome this problem is the use of subcell models, which means that on the basis of the knowledge of the analytical field behavior around small objects, one locally adapts the FDTD time-stepping equation. In this way the time step is dictated mainly by a coarse grid. In Ref. 9 a technique was presented that automatically generates such subcell models in the FDTD technique that can be used for arbitrarily shaped objects. Also, the memory requirements are kept small by reducing the number of internal variables in the subcell model by means of a reduced-order modeling (ROM) technique.

Another frequently used numerical method is the eigenmode expansion technique. This technique starts by slicing the structure into layers for which the index profile does not change in a given direction. For each layer, the fields are written as a sum of the so-called eigenmodes of that layer. The unknown expansion coefficients are obtained by the well-known mode-matching technique at the interfaces between the different layers. If a specific layer is frequently repeated, the computational complexity scales linearly or even logarithmically with the longitudinal dimension of the structure. By calculating the reflection matrix of a semi-infinite crystal, one can terminate the PC structure and avoid back reflections coming from abruptly terminated waveguides. However, the eigenmode expansion technique requires a discrete set of modes. Typically, this is achieved by enclosing the entire structure in a metal box. Unfortunately, this can create parasitic reflections. A better way is to make use of advanced boundary conditions, such as perfectly matched layers (PMLs).[10–12] This also speeds up the computation time, as the metal walls can now be placed much closer to the structure.

A third method is the multiple-scattering technique,[13–15] which is a rigorous semianalytical technique. In contrast to FDTD and the eigenmode expansion technique, this method exploits the fact that the cylinders have a circular cross section by using Bessel–Hankel functions, which are the "natural" modes for cylindrical objects, i.e., scalar cylindrical harmonics. As a consequence, only a few unknowns per cylinder are required. We will show that this method is not only limited to finite PC structures. By adding some extra rows of cylinders in the complex plane, one can efficiently avoid reflections.[16] However, with this method the solution of a linear system whose dimension scales linearly with the number of cylinders is required. With a direct solver the computational complexity scales as the cube of the number of cylinders.

In Sections 2, 3, and 4 the basic principles of the three simulation techniques are summarized, and some additional improvements over published results are pre-

sented. The main advantages and disadvantages of each method are also discussed. In Section 5 some PC filter structures are simulated, and the results obtained with the different methods are compared and discussed.

## 2. SEMIANALYTICAL TECHNIQUE

In this section a semianalytical technique for computing the scattering by a large number of circular dielectric or perfectly conducting (PEC) cylinders is described. First the total field is written as the sum of the incident field due to the source and the field scattered by the cylinders. To calculate this scattered field we introduce surface currents at the surface of each cylinder. For PEC cylinders, these currents correspond to the physical surface currents, but for dielectric cylinders these currents are fictitious. The scattered field is then written as the sum of the fields due to these currents.

### A. Field and Current Representation

At the surface of every cylinder $i$ (Fig. 1) we define unknown surface currents

$$J_z^i(\rho_i = a_i, \ \phi_i) = \sum_{m=-\infty}^{+\infty} \frac{I_m^i}{2\pi a_i} \exp(jm\phi_i), \qquad (1)$$

with $a_i$ the radius of cylinder $i$ and $(\rho_i, \ \phi_i)$ the local cylindrical coordinates of this cylinder. These currents are placed in an infinite, homogeneous medium with refractive index $n_{\text{ext}}$. The total electric field on the surface of cylinder $i$ can also be written as a Fourier series

$$E_z^i(\rho_i = a_i, \ \phi_i) = \sum_{p=-\infty}^{+\infty} e_p^i \exp(jp\phi_i), \qquad (2)$$

with

$$e_p^i = \frac{1}{2\pi} \int_{-\pi}^{\pi} E_z^i(\rho_i = a_i, \ \phi_i)\exp(-jp\phi_i)\mathrm{d}\phi_i. \qquad (3)$$

The total field $E_z^i(\rho_i = a_i, \ \phi_i)$ is the superposition of the following three contributions:

(i) the field caused by the surface current on cylinder $i$,

$$E_z^{ii} = \sum_{p=-\infty}^{+\infty} e_p^{ii} \exp(jp\phi_i), \qquad (4)$$
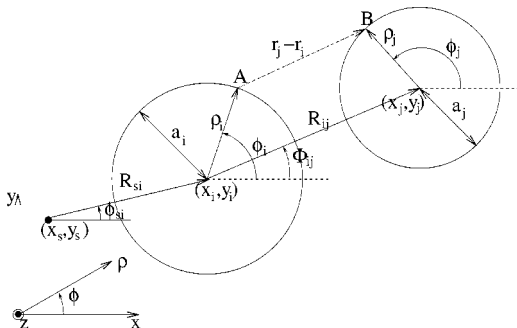


Fig. 1. Basic geometry and coordinate systems.

(ii) the field caused by the surface currents on the other cylinders,

$$E_z^{ji} = \sum_{p=-\infty}^{+\infty} \sum_{j\neq i} e_p^{ji} \exp(jp\phi_i); \qquad (5)$$

(iii) the field caused by the source,

$$E_z^{0i} = \sum_{p=-\infty}^{+\infty} e_p^{0i} \exp(jp\phi_i). \qquad (6)$$

One can easily verify that the first contribution is given by

$$e_p^{ii} = -\frac{\omega\mu_0}{4} H_p^{(2)}(ka_i)J_p(ka_i)I_p^i. \qquad (7)$$

To calculate the contribution $e_p^{ji}$, we express the field caused by the currents on cylinder $j$ in terms of the local coordinates of cylinder $i$ by using the addition theorem of the Hankel functions.[17] We find that

$$e_p^{ji} = -\frac{\omega\mu_0}{4} \sum_{m=-\infty}^{+\infty} H_{p-m}^{(2)}(kR_{ij})J_m(ka_j)J_p(ka_i)$$
$$\times \exp[j(m-p)\Phi_{ij}]I_m^j, \qquad (8)$$

with $R_{ij}$ and $\Phi_{ij}$, respectively, the distance and the angle between the centers of the two cylinders; see Fig. 1.

Again using the addition theorem of the Hankel functions, we can easily calculate the contribution of the source $e_p^{0i}$. For a line source situated at a point $(x_0, y_0)$, the field at a point on the surface of cylinder $i$ is given by

$$E_z^{0i}(a_i, \ \phi_i) = -\frac{\omega\mu_0}{4} H_0^{(2)}(kr_{0i})$$

$$= -\frac{\omega\mu_0}{4} H_0^{(2)}(k|\mathbf{R}_{0i} + \boldsymbol{\rho}_i|)$$

$$= -\frac{\omega\mu_0}{4} \sum_{n=-\infty}^{+\infty} (-1)^n H_n^{(2)}(kR_{0i})$$
$$\times J_n(ka_i)\exp[jn(\Phi_{0i} - \phi_i)], \qquad (9)$$

such that we obtain the source contribution

$$e_p^{0i} = -\frac{\omega\mu_0}{4}(-1)^p H_p^{(2)}(kR_{0i})J_p(ka_i)\exp(-jp\Phi_{0i}). \qquad (10)$$

### B. Boundary Impedance

For the case of perfectly conducting cylinders, the whole problem can be solved by requiring that the total electric field be zero on the surface of all cylinders. This in turn leads to a set of equations for the unknown surface currents $I_m^i$ in Eq. (1). For dielectric cylinders, internal fields have to be taken into account. Here we circumvent this problem by continuing to use the surface current of Eq. (1) as our only unknown quantity, but now an appropriate boundary impedance has to be introduced that relates the total external electric field to this current. For the calculation of this boundary impedance, we consider two situations (Fig. 2):
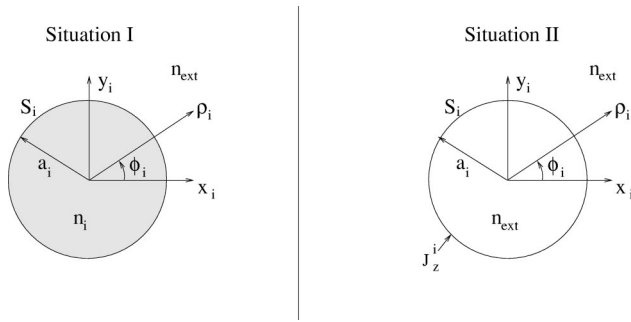
Fig. 2. Two situations for calculation of the boundary impedance.

1. The original situation with a dielectric cylinder with radius $a_i$ and refractive index $n_i$ placed in a homogeneous space with refractive index $n_{\text{ext}}$.

2. A homogeneous space with refractive index $n_{\text{ext}}$ but with unknown currents $J_z^i = \sum_{n=-\infty}^{+\infty} I_n^i \exp(jn\phi_i)$ placed on the now fictitious surface $S_i$ of cylinder $i$.

In the first situation the fields inside the dielectric cylinder are given by

$$E_z^I(\rho_i \leq a_i, \phi_i) = \sum_{n=-\infty}^{+\infty} A_n J_n(k_0 n_i \rho_i)\exp(jn\phi_i),$$
(11)

$$j\omega\mu_0 H_{\phi_i}^I(\rho_i \leq a_i, \phi_i) = k_0 n_i \sum_{n=-\infty}^{+\infty} A_n J_n'(k_0 n_i \rho_i)$$

$$\times \exp(jn\phi_i),$$
(12)

where $A_n$ are unknown coefficients. In the second situation the fields at $\rho_i = a_i^+$ are given by

$$E_z^{II}(a_i^+, \phi_i) = \sum_{n=-\infty}^{+\infty} B_n J_n(k_0 n_{\text{ext}} a_i)\exp(jn\phi_i),$$
(13)

$$j\omega\mu_0 H_{\phi_i}^{II}(a_i^+, \phi_i) = k_0 n_{\text{ext}} \sum_{n=-\infty}^{+\infty} B_n J_n'(k_0 n_{\text{ext}} a_i)\exp(jn\phi_i)$$

$$+ j\omega\mu_0 \sum_{-\infty}^{+\infty} \frac{I_n^i}{2\pi a_i}\exp(jn\phi_i).$$
(14)

We define the boundary admittance $Y_n^i = 1/Z_n^i$ as

$$\frac{I_n^i}{2\pi a_i} = Y_n^i e_n^{II}(a_i) = Y_n^i B_n J_n(k_0 n_{\text{ext}} a_i).$$
(15)

This boundary admittance can be determined by requiring that

$$E_z^I(a_i^-, \phi_i) = E_z^{II}(a_i^+, \phi_i),$$
(16)

$$H_{\phi_i}^I(a_i^-, \phi_i) = H_{\phi_i}^{II}(a_i^+, \phi_i).$$
(17)

This yields

A perfectly conducting cylinder corresponds to $\epsilon_i = \infty$ or $Z_n^i = 0$, as expected. The unknown surface currents are then determined by

$$E_z^i(a_i, \phi_i) = Z_n^i I_n^i,$$
(19a)

or

$$E_z^{\text{tot}}(a_i, \phi_i) - \sum_{n=-\infty}^{+\infty} Z_n^i I_n^i \exp(jn\phi_i) = 0.$$
(19b)

In practice, this infinite sum has to be truncated to a finite number of terms: $n$ going from $-N_m$ to $+N_m$. As will become clear in the examples, three terms for every cylinder (corresponding to $N_m = 1$) are usually sufficient. Similar formulas were derived in Refs. 13–15.

## C. Modeling Infinite Crystals with a Perfectly Matched Layer

When designing PC devices, one is usually not interested in back reflections coming from an abruptly terminated photonic crystal. Therefore it is advantageous to be able to model PC waveguides that are infinitely long in the propagation direction. This can be achieved, e.g., by incorporating an appropriate boundary condition. Recently such a boundary condition has been proposed for FDTD simulations, namely, a PC-based-PML.[18] The main difference from a regular PML boundary condition is that the PC structure is maintained in the PML. In Ref. 16 we introduced a similar boundary condition for integral-equation-like techniques. By exploiting the complex coordinate interpretation of a PML,[19,20] a PC structure can be terminated by adding a couple of periods in the complex plane. Although entering into the complex plane always causes a disturbance of the periodicity, the absorption in the PML region drastically reduces the reflections at the termination of the PC structure compared with a termination in real space. The remaining reflections due to the disturbance of the periodicity can be strongly reduced if the waveguide enters the complex plane smoothly. In Ref. 16 two different ways to enter the complex plane were compared, namely a "linear" PML and a "circular" PML. It was shown that the circular PML outperforms the linear PML.

## D. Advantages

The advantages of the semianalytical method are as follows:

1. Because this is a semianalytical technique, the accuracy is very much under control, which makes this technique well suited as a benchmark technique. No phase errors are introduced.

2. For finite structures this technique does not rely on an absorbing boundary condition.

$$Z_n^i = j\sqrt{\frac{\mu_0}{\epsilon_0}}\frac{J_n(k_0 n_{\text{ext}} a_i)J_n(k_0 n_i a_i)}{n_{\text{ext}}J_{n+1}(k_0 n_{\text{ext}} a_i)J_n(k_0 n_i a_i) - n_i J_{n+1}(k_0 n_i a_i)J_n(k_0 n_{\text{ext}} a_i)}.$$
(18)

3. This technique is suited for wires with arbitrary losses ranging from dielectric wires to perfectly conducting wires.

### E. Disadvantages
The disadvantages of the semianalytical method are as follows:

1. CPU time is proportional to $N^3$; however the number of unknowns $N$ will be much smaller than with mode matching.

2. The technique is limited to circular wires. Extension to arbitrary shapes is possible, but at significant extra cost.

## 3. VECTORIAL EIGENMODE EXPANSION

The general principles behind the vectorial eigenmode expansion method have already been described, e.g., in Refs. 11 and 12 and references therein. For clarity, we will briefly review the main principles behind the method, as well as clarify its advantages and disadvantages when applied to the modeling of photonic crystal structures. In the following sections we will extend the method to deal with a source placed inside a structure and with photonic crystals that extend infinitely in the propagation direction. CAMFR, our implementation of this model, is freely available from Ref. 21.

### A. Overview of Eigenmode Expansion
The main philosophy of the eigenmode expansion method is to divide the structure of interest into a number of layers in which the refractive-index profile does not change in the propagation or $z$ direction. If the geometry is not piecewise constant, a suitable staircase approximation can be chosen; see Fig. 3. Subsequently, the vectorial eigenmodes of these waveguide sections are calculated and are used as basis functions for a field expansion. At the interface between two different layers, mode matching is applied to derive the reflection and transmission matrices, which can be used to calculate the reflection and
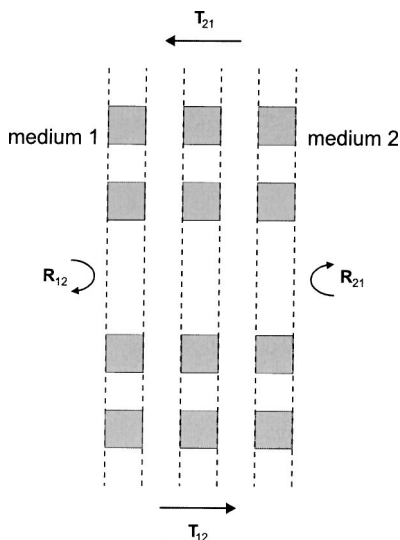


Fig. 3. Reflection and transmission of a layered medium.
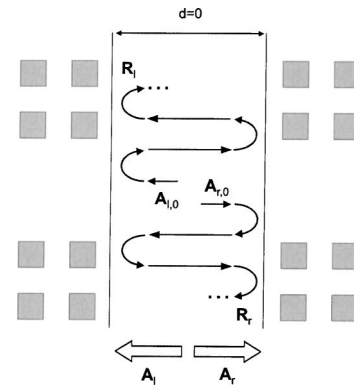


Fig. 4. Source inside a layered medium.

transmission matrices $\mathbf{R}_{12}$ and $\mathbf{T}_{12}$ of the entire structure. For an arbitrary incident field described by its expansion vector $\mathbf{A}_1$ in the eigenmodes, the reflected and transmitted fields are given by $\mathbf{R}_{12} \cdot \mathbf{A}_1$ and $\mathbf{T}_{12} \cdot \mathbf{A}_1$, respectively. Similar matrices $\mathbf{R}_{21}$ and $\mathbf{T}_{21}$ can be derived for incidence from the other side.

### B. Source Inside a Structure
The natural excitation of a structure in this formalism is an incident field expanded in eigenmodes and impinging on the structure from the outside. This field can even be a Bloch mode, which reduces the required computational domain, as no extra length of photonic crystal waveguide is needed to achieve an equilibrium field distribution. For a dipole current source as excitation, a longer waveguide would be needed to achieve this equilibrium. However, it is also possible to calculate the response to a current source (or a more general source) placed inside the structure, as will now be shown.

The plane which contains the source divides the structure into a left and a right part, of which we can calculate the reflection matrices $\mathbf{R}_l$ and $\mathbf{R}_r$ (Fig. 4). The exact field pattern emitted by this source is arbitrary; only its expansion coefficients need to be known. In general, the source will radiate in both directions (right–forward and left–backward), so it is fully characterized by two expansion vectors $\mathbf{A}_{r,0}$ and $\mathbf{A}_{l,0}$.

Let us concentrate for the moment on the source term $\mathbf{A}_{r,0}$. This field distribution will keep on bouncing back and forth between the right and left part of the structure such that the equilibrium forward field distribution just to the right of the source will be

$$\mathbf{A}_{r,0} + \mathbf{R}_l \cdot \mathbf{R}_r \cdot \mathbf{A}_{r,0} + \mathbf{R}_l \cdot \mathbf{R}_r \cdot \mathbf{R}_l \cdot \mathbf{R}_r \cdot \mathbf{A}_{r,0} + \cdots. \quad (20)$$

We can write this as

$$\sum_{i=0}^{\infty} (\mathbf{R}_l \cdot \mathbf{R}_r)^i \cdot \mathbf{A}_{r,0}. \quad (21)$$

This sum converges to

$$(\mathbf{I} - \mathbf{R}_l \cdot \mathbf{R}_r)^{-1} \cdot \mathbf{A}_{r,0}. \quad (22)$$

The other source term $\mathbf{A}_{l,0}$ also contributes to the total forward field. After reflecting at the left part, it goes through the same sequence of reflections as in relation (20). Therefore the total forward equilibrium field can be written as

$$\mathbf{A}_\text{r} = (\mathbf{I} - \mathbf{R}_\text{l} \cdot \mathbf{R}_\text{r})^{-1} \cdot (\mathbf{A}_{\text{r},0} + \mathbf{R}_\text{l} \cdot \mathbf{A}_{\text{l},0}). \qquad (23)$$

Similarly, the total backward field just to the left of the source is

$$\mathbf{A}_\text{l} = (\mathbf{I} - \mathbf{R}_\text{r} \cdot \mathbf{R}_\text{l})^{-1} \cdot (\mathbf{A}_{\text{l},0} + \mathbf{R}_\text{r} \cdot \mathbf{A}_{\text{r},0}). \qquad (24)$$

Using these field distributions as excitations for, respectively, the right and the left part of the structure, we can calculate the total field at an arbitrary position. This completely characterizes the response of the structure to the source.

For the specific case of a dipole current source $\mathbf{J}_0 \delta(\mathbf{r} - \mathbf{r}_0)$, we can calculate the source terms $\mathbf{A}_{\text{r},0}$ and $\mathbf{A}_{\text{l},0}$ based on the Lorentz reciprocity theorem[22] as

$$-2A_{\text{l},m} = \mathbf{J}_0 \cdot \mathbf{E}_{\text{r},m}(\mathbf{r}_0), \qquad (25)$$

$$-2A_{\text{r},m} = \mathbf{J}_0 \cdot \mathbf{E}_{\text{l},m}(\mathbf{r}_0). \qquad (26)$$

Here $m$ is the index of the mode.

### C. Modeling Infinite Crystals

In the eigenmode expansion formalism another more exact method can be used to reduce reflections. That is, it is possible to calculate the reflection matrix $\mathbf{R}_\infty$ of a semi-infinite crystal and then to use this matrix to terminate the structure in the propagation direction.

To calculate this matrix $\mathbf{R}_\infty$ we first calculate the Bloch modes of the infinite crystal by solving the following generalized eigenvalue problem containing the scattering matrices of the basic period[23,24]:

$$\begin{bmatrix} \mathbf{T}_{12} & \mathbf{R}_{21} \\ \mathbf{0} & \mathbf{I} \end{bmatrix} \begin{pmatrix} \mathbf{F}_1 \\ q\mathbf{B}_1 \end{pmatrix} = q \begin{bmatrix} \mathbf{I} & \mathbf{0} \\ \mathbf{R}_{12} & \mathbf{T}_{21} \end{bmatrix} \begin{pmatrix} \mathbf{F}_1 \\ q\mathbf{B}_1 \end{pmatrix}. \qquad (27)$$

Here $\mathbf{F}_1$ and $\mathbf{B}_1$ are the forward and backward components of the Bloch mode at the left-hand side of the unit cell, and $q$ is related to the Bloch vector $\beta$ by $q = \exp(-i\beta d)$, with $d$ the length of the basic period. Equation (27) is more stable than more traditional methods based on calculating eigenvectors of the transfer matrix, because it does not contain any matrix inversions. For higher-order evanescent modes, the corresponding diagonal elements in $\mathbf{T}_{12}$ and $\mathbf{T}_{21}$ are close to zero. Therefore $\mathbf{T}_{12}$ and $\mathbf{T}_{21}$ are close to singular and cannot be inverted in a stable way. It is this inversion that Eq. (27) avoids.

For $N$ modes retained in the series expansion, this method will give rise to $2N$ solutions, half of which are Bloch modes with a forward flux, the other half with a backward flux. We retain only those with forward flux and arrange their field profiles as column vectors in two matrices $\mathbf{F}^+$ and $\mathbf{B}^+$. We can now calculate the reflection matrix of the semi-infinite stack as

$$\mathbf{R}_\infty = \mathbf{B}^+ \cdot \mathbf{F}^{+^{-1}}, \qquad (28)$$

which is intuitively plausible as being a generalized ratio between a backward and a forward field. A similar idea was already put forward in Ref. 25.

### D. Advantages

The advantages of the vectorial eigenmode expansion are the following:

1. The calculation time is linear in the number of layers, and not in the total length of the structure, as the propagation through layers can be handled analytically.

2. In modeling structures with a finite number of repetitions of a basic period (as is common in PC devices), calculation time for the scattering matrices is logarithmic in the number of periods rather than linear.[11]

3. PML boundary conditions[26,27] can be introduced trivially by allowing the cladding thickness to take on complex values.[20] In this way, structures with radiation losses can be handled.

4. Abruptly terminating a photonic crystal will give rise to unwanted reflections from the end face. In eigenmode expansion it is possible to calculate analytically crystals that are infinite in the propagation direction, thereby solving this problem.

### E. Disadvantages

The disadvantages of eigenmode expansion are the following:

1. This technique behaves less advantageouly if there is no repetition of layers, which would be the case when considering irregular structures.

2. For curved nonrectangular objects, many layers are needed.

3. This technique relies on an absorbing boundary condition.

4. Considerable performance is lost if the structure is excited by waveguides that run along different directions.

## 4. THE SUBDOMAIN, FINITE-DIFFERENCE TIME-DOMAIN METHOD

The FDTD technique has often been used to analyze PC structures.[28–30] One of the problems in doing so is the fine grid needed to capture the shape of the periodic unit cells. In Ref. 9 a scheme was developed to automatically generate new FDTD update equations for objects that are smaller than the grid step size. With this technique the simulation of PC structures by FDTD can be enhanced dramatically. Here we will give a brief summary of the technique presented in Ref. 9 and at some point improve it in two respects.

Consider a part of a TM FDTD grid as shown in Fig. 5. We consider a local fine grid inside a contour $C$ that encloses the small object that will be periodically repeated when used in a PC structure. Outside the contour $C$ we use a coarse grid. The refinement ratio $r$ is defined as $r = \Delta_\text{c}/\Delta_\text{f}$. In the fine grid the FDTD equations can be written as

$$\epsilon \frac{dE_z^{i+1/2,j+1/2}(t)}{dt} = \frac{H_y^{i+1,j+1/2}(t) - H_y^{i,j+1/2}(t)}{\Delta_\text{f}}$$

$$- \frac{H_x^{i+1/2,j+1}(t) - H_x^{i+1/2,j}(t)}{\Delta_\text{f}}, \qquad (29)$$

$$\mu_0 \frac{dH_y^{i,j+1/2}(t)}{dt} = \frac{E_z^{i+1/2,j+1/2}(t) - E_z^{i-1/2,j+1/2}(t)}{\Delta_{\mathrm{f}},}$$
(30)

$$\mu_0 \frac{dH_x^{i+1/2,j}(t)}{dt} = -\frac{E_z^{i+1/2,j+1/2}(t) - E_z^{i+1/2,j-1/2}(t)}{\Delta_{\mathrm{f}},}$$
(31)

where standard FDTD index notation was used and where $\Delta_{\mathrm{f}}$ is the fine mesh grid step. In these equations time is still kept continuous. Taking all these equations together for all field variables inside the contour $C$ yields the following system of first-order equations

$$\begin{bmatrix} \epsilon_0 \mathbf{D}_\epsilon & \mathbf{0} \\ \mathbf{0} & \mu_0 \mathbf{I} \end{bmatrix} \begin{pmatrix} \dot{\mathbf{e}} \\ \dot{\mathbf{h}} \end{pmatrix} = -\frac{1}{\Delta_{\mathrm{f}}} \begin{bmatrix} \mathbf{0} & \mathbf{K} \\ -\mathbf{K}^T & \mathbf{0} \end{bmatrix} \begin{pmatrix} \mathbf{e} \\ \mathbf{h} \end{pmatrix} + \frac{1}{\Delta_{\mathrm{f}}} \begin{pmatrix} \mathbf{0} \\ \mathbf{B} \end{pmatrix} \mathbf{u}$$

$$\mathbf{y} = \begin{bmatrix} \mathbf{0} & \mathbf{L}^T \end{bmatrix} \begin{pmatrix} \mathbf{e} \\ \mathbf{h} \end{pmatrix},$$
(32)

with $\mathbf{e}$ a vector with all variables $E_z^{i+1/2,j+1/2}$ inside $C$ and $\mathbf{h}$ a vector with all variables $H_x^{i+1/2,j+1}$ and $H_y^{i+1,j+1/2}$ inside or on $C$; $\dot{\mathbf{e}}$ and $\dot{\mathbf{h}}$ denote the time derivatives of $\mathbf{e}$ and



Fig. 5. A fine and a coarse grids with refinement ratio, $r = \Delta_{\mathrm{c}}/\Delta_{\mathrm{f}} = 3$.

$\mathbf{h}$, and $\mathbf{u}$ is a vector with the variables $E_z^{i+1/2,j+1/2}$ just outside the fine grid as if the fine grid had been extended by one row of cells. The vector $\mathbf{y}$ contains the components $H_x^{i+1/2,j+1}$ and $H_y^{i+1,j+1/2}$ on the boundary $C$. The matrices $\mathbf{K}$ and $\mathbf{B}$ are sparse matrices with nonzero elements equal to $\pm 1$. The matrix $\mathbf{D}_\epsilon$ is a diagonal matrix with the relative permittivities in each cell. The matrix $\mathbf{L}$ contains a few elements equal to 1 in order to pick the subset $\mathbf{y}$ from $\mathbf{x}$. Now we have to connect the fine grid variables $\mathbf{y}$ and $\mathbf{u}$ to the coarse grid variables $\mathbf{Y}$ and $\mathbf{U}$. This can be done in many different ways.[9] In general we can write

$$\mathbf{u} = \mathbf{A}\mathbf{U},$$
(33)

$$\mathbf{Y} = \mathbf{D}\mathbf{y},$$
(34)

with $\mathbf{U}$ the $E_z^{i+1/2,j+1/2}$ variables of the coarse grid just outside $C$ and with $\mathbf{Y}$ the $H_x^{i+1/2,j+1}$ and $H_y^{i+1,j+1/2}$ variables of the coarse grid on $C$. In this way we can recast system (32) as

$$\begin{bmatrix} \epsilon_0 \mathbf{D}_\epsilon & \mathbf{0} \\ \mathbf{0} & \mu_0 \mathbf{I} \end{bmatrix} \begin{pmatrix} \dot{\mathbf{e}} \\ \dot{\mathbf{h}} \end{pmatrix} = -\frac{1}{\Delta_{\mathrm{f}}} \begin{bmatrix} \mathbf{0} & \mathbf{K} \\ -\mathbf{K}^T & \mathbf{0} \end{bmatrix} \begin{pmatrix} \mathbf{e} \\ \mathbf{h} \end{pmatrix} + \frac{1}{\Delta_{\mathrm{f}}} \begin{pmatrix} \mathbf{0} \\ \mathbf{B}' \end{pmatrix} \mathbf{U}$$

$$\mathbf{Y} = \begin{bmatrix} \mathbf{0} & \mathbf{L}'^T \end{bmatrix} \begin{pmatrix} \mathbf{e} \\ \mathbf{h} \end{pmatrix},$$
(35)

with $\mathbf{B}' = \mathbf{B}\mathbf{A}$ and $\mathbf{L}' = \mathbf{L}\mathbf{D}^T$.

In the next step we will use a ROM technique,[31] characterized by an order of approximation $q$, to reduce the size of the vectors $\mathbf{e}$ and $\mathbf{h}$ drastically while still retaining the same dynamic behavior of system (35) up to a certain frequency. The result is

$$\begin{bmatrix} \epsilon_0 \mathbf{I} & \mathbf{0} \\ \mathbf{0} & \mu_0 \mathbf{I} \end{bmatrix} \begin{pmatrix} \dot{\mathbf{x}}_1 \\ \dot{\mathbf{x}}_2 \end{pmatrix} = -\frac{1}{\Delta_{\mathrm{f}}} \begin{bmatrix} \mathbf{0} & \widetilde{\mathbf{K}} \\ -\widetilde{\mathbf{K}}^T & \mathbf{0} \end{bmatrix} \begin{pmatrix} \mathbf{x}_1 \\ \mathbf{x}_2 \end{pmatrix} + \frac{1}{\Delta_{\mathrm{f}}} \begin{pmatrix} \mathbf{0} \\ \widetilde{\mathbf{B}} \end{pmatrix} \mathbf{U}$$

$$\mathbf{Y} = \begin{bmatrix} \mathbf{0} & \overline{\mathbf{L}}^T \end{bmatrix} \begin{pmatrix} \mathbf{x}_1 \\ \mathbf{x}_2 \end{pmatrix}.$$
(36)

We can enhance this further by diagonalizing the full matrix $\widetilde{\mathbf{K}}$ using a singular-value decomposition:

$$\widetilde{\mathbf{K}} = \widetilde{\mathbf{U}}^T \boldsymbol{\Sigma} \widetilde{\mathbf{V}}.$$
(37)

By changing the variables $\mathbf{z}_1 = \widetilde{\mathbf{U}}\mathbf{x}_1$ and $\mathbf{z}_2 = \widetilde{\mathbf{U}}\mathbf{x}_2$, we rewrite system (36) as

$$\begin{bmatrix} \epsilon_0 \mathbf{I} & \mathbf{0} \\ \mathbf{0} & \mu_0 \mathbf{I} \end{bmatrix} \begin{pmatrix} \dot{\mathbf{z}}_1 \\ \dot{\mathbf{z}}_2 \end{pmatrix} = -\frac{1}{\Delta_{\mathrm{f}}} \begin{bmatrix} \mathbf{0} & \boldsymbol{\Sigma} \\ -\boldsymbol{\Sigma}^T & \mathbf{0} \end{bmatrix} \begin{pmatrix} \mathbf{z}_1 \\ \mathbf{z}_2 \end{pmatrix} + \frac{1}{\Delta_{\mathrm{f}}} \begin{pmatrix} \mathbf{0} \\ \widetilde{\mathbf{V}}\widetilde{\mathbf{B}} \end{pmatrix} \mathbf{u}$$

$$\mathbf{y} = \begin{bmatrix} \mathbf{0} & \widetilde{\mathbf{L}}^T \widetilde{\mathbf{V}}^T \end{bmatrix} \begin{pmatrix} \mathbf{z}_1 \\ \mathbf{z}_2 \end{pmatrix}.$$
(38)

This diagonalization was not introduced in Ref. 9. The FDTD iteration process now proceeds as follows. Suppose everything is known until time step $t = (n - 1/2)\Delta_t$:

• First, we update the electric fields outside $C$ in the coarse grid with the regular equation:
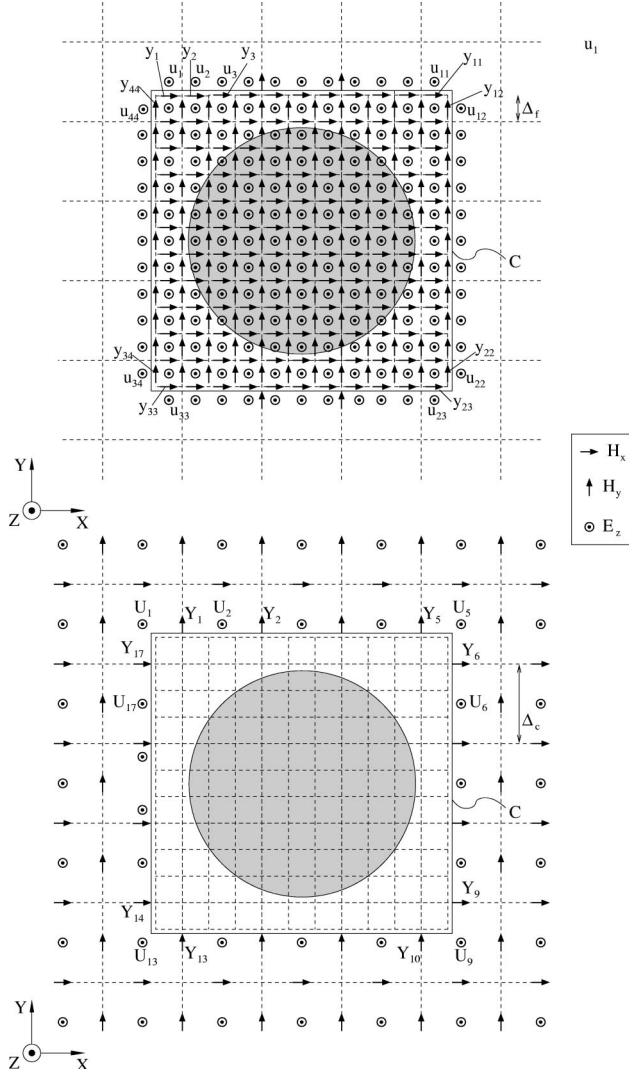
$$E_z^{i+1/2,j+1/2}(n) = E_z^{i+1/2,j+1/2}(n-1)$$

$$+ \frac{\Delta_t}{\epsilon \Delta_c}[H_y^{i+1,j+1/2}(n-1/2)$$

$$- H_y^{i,j+1/2}(n-1/2)]$$

$$- \frac{\Delta_t}{\epsilon \Delta_c}[H_x^{i+1/2,j+1}(n-1/2)$$

$$- H_x^{i+1/2,j}(n-1/2)], \qquad (39)$$

with $\Delta_t$ the time step and $\Delta_c$ the coarse grid step. Note that some of the magnetic fields on the right-hand side are extracted from $\mathbf{y}(n-1/2)$ when $E_z^{i+1/2,j+1/2} \in \mathbf{u}$.

Second, we update the magnetic fields outside $C$ with the regular equations:

$$H_y^{i,j+1/2}(n+1/2) = H_y^{i,j+1/2}(n-1/2)$$

$$+ \frac{\Delta_t}{\mu \Delta_c}[E_z^{i+1/2,j+1/2}(n)$$

$$- E_z^{i-1/2,j+1/2}(n)], \qquad (40)$$

and similarly for the $H_x$ components.

Third, we discretize state-space system (38) using an explicit scheme. The variables $\mathbf{z}_1$ are discretized around the same moment in time as the electric field variables, say $t = n\Delta_t$. The variables $\mathbf{z}_2$ are discretized around the same moment in time as the magnetic field variables, a half time step later than the electric field variables: $t = (n+1/2)\Delta_t$. This results in the following equations:

$$\mathbf{z}_1|^{n+1/2} = \mathbf{z}_1|^{n-1/2} - \frac{\Delta_t}{\epsilon_0 \Delta_f} \mathbf{\Sigma z}_2|^n, \qquad (41a)$$

$$\mathbf{z}_2|^{n+1} = \mathbf{z}_1|^n + \frac{\Delta_t}{\mu_0 \Delta_f} \mathbf{\Sigma}^T \mathbf{z}_1|^{n+1/2}$$

$$+ \frac{\Delta_t}{\mu_0 \Delta_f} \widetilde{\mathbf{V}} \widetilde{\mathbf{B}} \mathbf{u}|^{n+1/2}, \qquad (41b)$$

$$\mathbf{y}|^{n+1} = \widetilde{\mathbf{L}}^T \widetilde{\mathbf{V}}^T \mathbf{z}_2|^{n+1}. \qquad (41c)$$

It can be shown that this scheme is stable for

$$\Delta_t < 2/c_0 \sigma, \qquad (42)$$

with $\sigma$ the largest eigenvalue of $\widetilde{\mathbf{K}}$ or the largest element of $\mathbf{\Sigma}$. This is an explicit scheme and differs from the implicit scheme proposed in Ref. 9. Although the implicit scheme[9] is unconditionally stable, it suffers from late-time instabilities. The new scheme of Eqs. (41) has the stability condition of Eq. (42) related to it, and numerical experiments show that choosing

$$\Delta_t < \min\{2/c_0 \sigma, \ \Delta_c/\sqrt{2}c_0\} \qquad (43)$$

results in a stable iteration scheme.

It is clear that model (38) can be calculated once and for all. Therefore the time-consuming ROM and singular-value decomposition are performed in advance and depend only on the shape of the cell that is repeated in the photonic crystal.
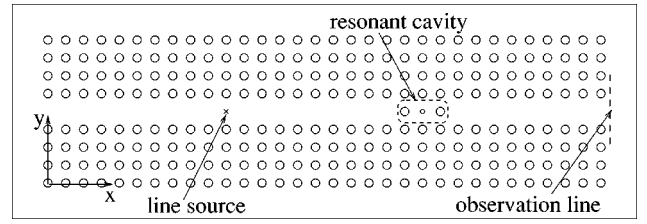


Fig. 6. Geometry of the PC structure used for comparison of the three techniques.

### A. Advantages
The advantages of the FDTD method are the following:

1. The CPU time and memory requirements scale linearly with the number of cylinders.
2. This approach is not limited to circular cylinders, and the numerical complexity does not increase when the shape of the periodic objects changes.
3. The technique yields results over a wide frequency range in a single run.

### B. Disadvantages
Disadvantages of the FDTD method are as follows:

1. The accuracy is more difficult to control.
2. The technique relies on absorbing boundary conditions.
3. FDTD in general suffers from the accumulation of phase errors for larger structures, which could lead to a change in resonance frequencies.
4. If there are many objects that are not repeated, this technique becomes costly in CPU time and memory.

## 5. EXAMPLES

In this section the PC structure shown in Fig. 6 is simulated with the three methods described in Sections 2, 3, and 4. The basic structure is a PC waveguide with a unit cell consisting of four dielectric cylinders at each side of the waveguide channel. This channel is actually formed by removing one row of cylinders. The radius of the cylinders of refractive index $n$ is $0.18a$, with $a$ the lattice constant, and they are placed in air. In the PC waveguide a resonant cavity is created by adding two or three cylinders. Because of this resonant cavity, the structure behaves as a filter: Only a small band around a certain frequency will be transmitted. Both finite and infinite PC structures are simulated. From this the effect of the reflections at the end surfaces of the PC waveguide becomes clear.

The finite PC waveguide consists of 32 unit cells. These unit cells are numbered from 1 to 32. The two cylinders of the resonant cavity are placed in the middle of rows 21 and 23 as shown in Fig. 6. A line source is placed in the middle of unit cell 11. The transmission spectrum $T(f)$ of this finite structure is calculated as follows. The energy flux $\Phi = \iint_S [\mathbf{E} \times \mathbf{H}^*] \cdot \mathbf{u}_n dS$, with $\mathbf{u}_n$ the unit vector in the direction of propagation, is calculated at the outlet of the PC structure. This is done by integration along a line situated at a distance $a/2$ from the outlet of the waveguide (Fig. 6). This flux is calculated for two situations: for the filter structure ($\Phi_{\text{filt}}$) and for the

waveguide without a resonant cavity ($\Phi_{wg}$). The transmission spectrum $T(f)$ is defined by

$$T(f) = \frac{\Phi_{\text{filt}}}{\Phi_{\text{wg}}} \qquad (44)$$

In the FDTD simulations the electric and magnetic fields are available only in discrete points that are determined by the coarse grid used. Consequently, the electric and magnetic fields are not known at the same points. To calculate the energy flux, linear interpolation for the magnetic fields is used. The transmission spectrum for the finite PC filter is given in Figs. 7 and 8 in the frequency range from $f = 0.36(c/a)$ to $f = 0.42(c/a)$ for $n = 3.4$ and $n = 2.83$, respectively. In the semianalytical technique, three unknowns per cylinder are used, which corresponds to $N_m = 1$ in Eq. (2). For the FDTD simulations, the refinement ratio $r$ is chosen to be 9 and a ROM technique with approximation order $q = 1$ is used. The time step is $0.056(a/c)$. The thickness of the layers used in the vectorial eigenmode expansion technique is $\Delta = a/20$. Excellent agreement among the three methods is observed. Note that because of reflections at the end surfaces, $T(f)$ as defined in Eq. (44) can become larger than 1.

For the infinite structures, the relative position of the line source, the cavity, and the observation points remains the same as for the finite structure. In the simulations with the semianalytical method of Section 2, a circular PML region with seven extra unit cells is added before and after the photonic crystal structure.[16] The $x$ coordinates of these cylinders are made complex according to a circle with radius $R = 10a$. For the PML region after the PC waveguide we can write

$$x_n^{\text{re}} = x_0 + R \sin n\alpha, \qquad (45)$$

$$x_n^{\text{im}} = -R(1 - \cos n\alpha), \qquad (46)$$

with $\alpha = 2 \arcsin(a/2R)$ and $x_0$ the $x$ coordinate of the last row in the PC waveguide before the PML. For the simulations with the subdomain FDTD method no extra boundary condition is added, but a very long waveguide with 100 extra unit cells before and after the original finite waveguide is calculated. In this way, the pulse that is transmitted through the resonant cavity can be easily
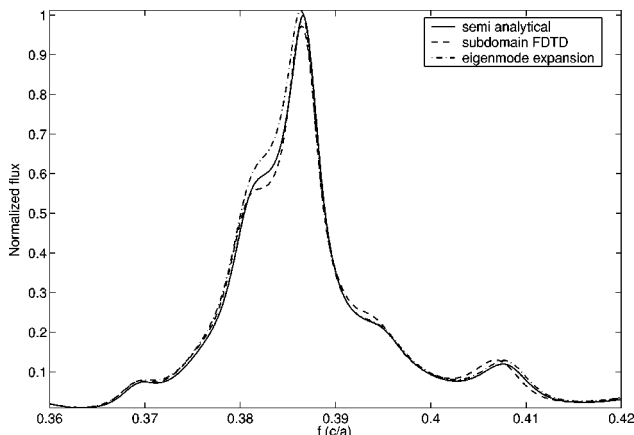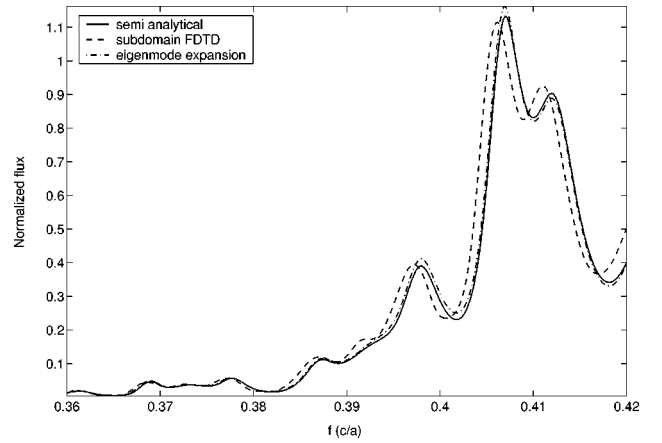
Fig. 8. Transmission through the finite filter structure, with $n = 2.83$.
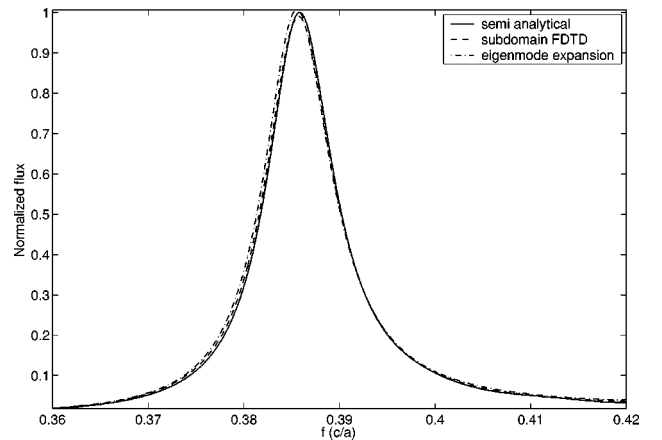
Fig. 9. Transmission through the infinite filter structure, with $n = 3.4$.

separated from the pulse that is reflected by the end surface of the PC waveguide. The transmission spectra for the infinite structures with the same parameters as in the finite case are given in Figs. 9 and 10. When one compares these results with the previous ones, it becomes clear that the reflections on the end surfaces have a rather strong influence on the behavior of the structure, as could be expected. The results also show that the complex coordinate technique to terminate the waveguide in the semianalytical technique works well. Note that $T(f)$ is now always smaller than 1. In Fig. 11 the electric field at the observation line is shown for the infinite PC waveguide with $n = 3.4$ at a frequency of $f = 0.36(c/a)$ and this for the three methods. Because the implementation of the source is not exactly the same for the frequency-domain techniques as for the time-domain technique, this electric field is normalized to its value at the center of the waveguide channel.

The central frequency of the filter can be tuned by placing an extra cylinder with a different radius and–or index of refraction in the middle of the cavity. We simulated the infinite PC structure with an extra rod with radius $r/4 = 0.045a$ but with the same index of refraction as the "regular" cylinders. For $n = 3.4$, the difference between the three schemes now becomes larger. This is due to the

Fig. 7. Transmission through the finite filter structure, with $n = 3.4$.

staircase approximation used in the FDTD and in the vec-
torial eigenmode expansion technique.   This shows that
the discretization used in the FDTD and in the vectorial
eigenmode expansion technique has to be chosen very fine
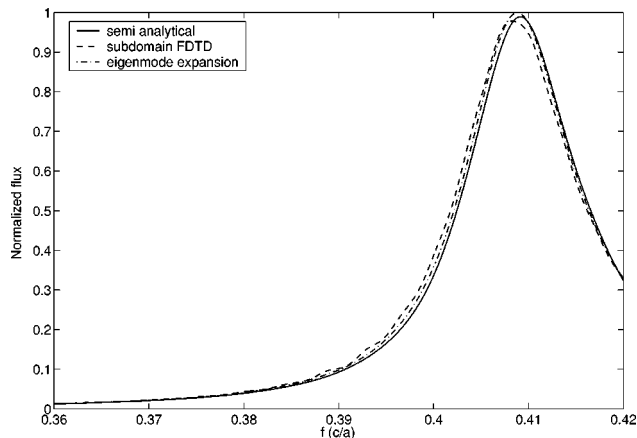


Fig. 10.   Transmission through the infinite filter structure, with
$n = 2.83$.
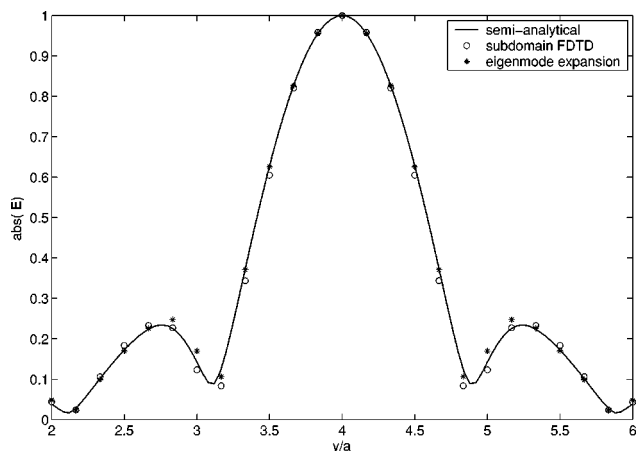


Fig. 11.   Electric field at the observation line shown in Fig. 6 for
an infinite waveguide, with $n = 3.4$ and $f = 0.36c/a$.
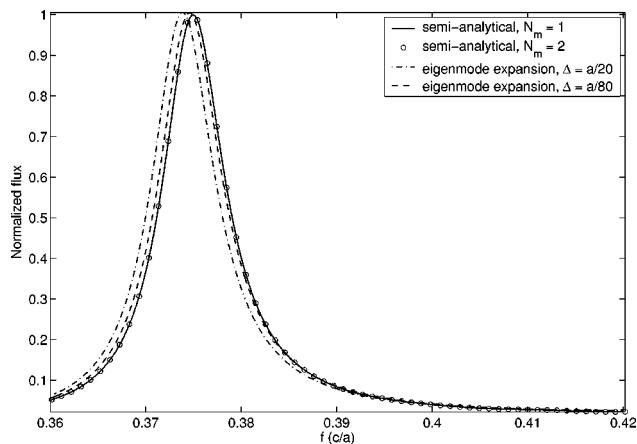


Fig. 12.   Transmission through the infinite filter structure with
one extra rod, with $n = 3.4$; comparison of the vectorial eigen-
mode expansion technique with the semianalytical technique.
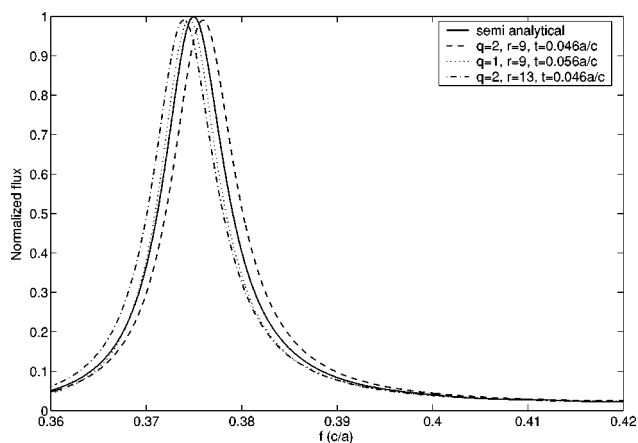


Fig. 13.   Transmission through the infinite filter structure with
one extra rod, with $n = 3.4$; comparison of the subdomain FDTD
technique with the semianalytical technique.
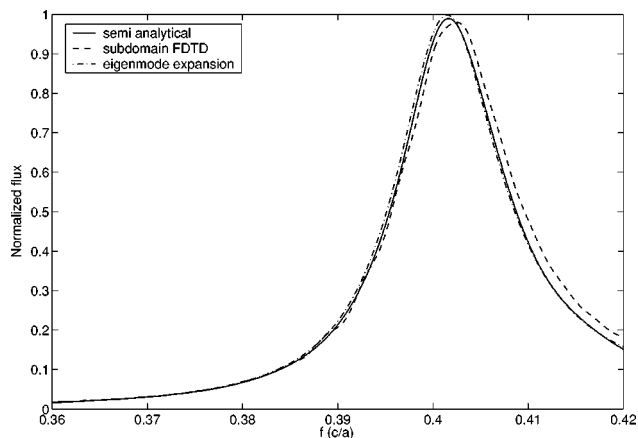


Fig. 14.   Transmission through the infinite filter structure with
one extra rod, with $n = 2.83$.

for accurate results.   In Fig. 12, we show on the one hand
that three unknowns are indeed sufficient in the semiana-
lytical technique and on the other hand that the results
for the vectorial eigenmode expansion technique converge
toward those of the semianalytical technique if the grid
size is decreased.   This finer grid has to be used only in
the region of the PC filter that contains the extra rod.
For the other parts of the structure a coarser grid still suf-
fices.   The accuracy of the FDTD subdomain technique
can be adjusted with three parameters:   the refinement
ratio $r$, the order of approximation $q$, and the time step
$\Delta_t$.   In Fig. 13, the transmission spectrum $T(f)$ of the
same PC filter as studied in Fig. 12 is shown for several
combinations of these parameters.   It is clear that it is
not so obvious to predict which combination will yield the
most accurate results, as was already mentioned in Sec-
tion 4.   In Fig. 14 the transmission spectrum is shown for
the infinite filter structure with one extra rod for the situ-
ation where $n = 2.83$.

## 6.   CONCLUSIONS

We have presented and compared three techniques for the
efficient simulation of two-dimensional PC structures:   a

semianalytical multiple-scattering technique, a vectorial eigenmode expansion technique, and a FDTD-ROM technique. The semianalytical technique yields accurate reference results, the vectorial eigenmode expansion technique is very fast, and the FDTD-ROM technique can give results over a wide frequency band in a single run.

## ACKNOWLEDGMENTS

## REFERENCES

1. J. D. Joannopoulos, R. D. Meade, and J. N. Winn, *Photonic Crystals, Molding the Flow of Light* (Princeton U. Press, Princeton, N.J., 1995).
2. A. Mekis, J. C. Chen, I. Kurland, S. Fan, P. R. Villeneuve, and J. D. Joannopoulos, "High transmission through sharp bends in photonic crystal waveguides," Phys. Rev. Lett. **77**, 3787–3790 (1996).
3. A. Chutinan and S. Noda, "Waveguides and waveguide bends in two-dimensional photonic crystal slabs," Phys. Rev. B **62**, 4488–4492 (2000).
4. H. Benisty, C. Weisbuch, M. Agio, M. Kafesaki, C. M. Soukoulis, M. Qiu, M. Swillo, A. Karlsson, B. Jaskorzynska, A. Talneau, J. Moosburger, M. Kamp, A. Forchell, R. Ferrini, R. Houdré, and U. Oesterle, "Models and measurements for the transmission of submicron-width waveguide bends defined in two-dimensional photonic crystals," IEEE J. Quantum Electron. **38**, 770–784 (2002).
5. O. Painter, R. K. Lee, A. Scherer, A. Yariv, J. D. O'Brien, P. D. Dapkus, and I. Kim, "Two-dimensional photonic bandgap defect mode laser," Science **284**, 1819–1821 (1999).
6. M. Koshiba, "Wavelength division multiplexing and demultiplexing with photonic crystal waveguide couplers," J. Lightwave Technol. **19**, 1970–1975 (2001).
7. C. Jin, S. Han, X. Meng, B. Cheng, and D. Zhang, "Demultiplexer using directly resonant tunneling between point defects and waveguides in a photonic crystal," J. Appl. Phys. **91**, 4771–4773 (2002).
8. S. Boscolo, M. Midrio, and C. S. Someda, "Coupling and decoupling of electromagnetic waves in parallel 2-D photonic crystal waveguides," IEEE J. Quantum Electron. **38**, 47–53 (2002).
9. B. Denecker, F. Olyslager, L. Knockaert, and D. De Zutter, "Generation of FDTD subcell equations by means of reduced order modeling," IEEE Trans. Antennas Propag. **51**, 1806–1817 (2003).
10. H. Derudder, D. De Zutter, and F. Olyslager, "A new way to analyse waveguide discontinuities using perfectly matched layers," Electron. Lett. **34**, 2138–2140 (1998).
11. P. Bienstman and R. Baets, "Optical modeling of photonic crystals and VCSELs using eigenmode expansion and perfectly matched layers," Opt. Quantum Electron. **33**, 327–341 (2001).
12. P. Bienstman and R. Baets, "Advanced boundary conditions for eigenmode expansion models," Opt. Quantum Electron. **34**, 523–540 (2002).
13. A. Z. Elsherbeni and A. A. Kishk, "Modelling of cylindrical objects by circular dielectric and conducting cylinders," IEEE Trans. Antennas Propag. **40**, 96–99 (1992).
14. A. Z. Elsherbeni, "A comparative study of two-dimensional multiple scattering techniques," Radio Sci. **29**, 1023–1033 (1994).
15. G. Tayeb and D. Maystre, "Rigorous theoretical study of finite-size two-dimensional photonic crystals doped by microcavities," J. Opt. Soc. Am. A **14**, 3323–3332 (1997).
16. D. Pissoort and F. Olyslager, "Termination of periodic waveguides by PMLs in time-harmonic integral equation-like techniques," IEEE Antennas Wire. Propag. Lett. **2**, 281–284 (2003).
17. W. Magnus, F. Oberhettinger, and R. P. Soni, *Formulas and Theorems for the Special Functions of Mathematical Physics* (Springer-Verlag, Berlin, 1966).
18. M. Koshiba, Y. Tsuji, and S. Sasaki, "High-performance absorbing boundary conditions for photonic crystal waveguide simulations," IEEE Microw. Wirel. Compon. Lett. **11**, 152–154 (2001).
19. W. C. Chew and W. H. Weedon, "A 3D perfectly matched medium from modified Maxwell's equations with stretched coordinates," Microwave Opt. Technol. Lett. **7**, 599–604 (1994).
20. W. C. Chew, J. M. Jin, and E. Michielssen, "Complex coordinate stretching as a generalized absorbing boundary condition," Microwave Opt. Technol. Lett. **15**, 363–369 (1997).
21. http://camfr.sourceforge.net.
22. H. Derudder, F. Olyslager, and D. De Zutter, "An efficient series expansion for the 2-D Green's function of a microstrip substrate using perfectly matched layers," IEEE Microw. Guid. Wave Lett. **9**, 505–507 (1999).
23. K. C. Huang, P. Bienstman, J. D. Joannopoulos, K. A. Nelson, and S. Fan, "Phonon-polariton excitations in photonic crystals," Phys. Rev. B **68**, 075209 (2003).
24. Q. Cao, P. Lalanne, and J. P. Hugonin, "Stable and efficient Bloch-mode computational method for one-dimensional grating waveguides," J. Opt. Soc. Am. A **19**, 335–338 (2002).
25. J. Ĉtyroký, S. Helfert, and R. Pregla, "Analysis of a deep waveguide Bragg grating," Opt. Quantum Electron. **30**, 343–358 (1998).
26. J.-P. Bérenger, "A perfectly matched layer for the absorption of electromagnetic waves," J. Comput. Phys. **114**, 185–200 (1994).
27. H. Derudder, F. Olyslager, D. De Zutter, and S. Van den Berghe, "Efficient mode-matching analysis of discontinuities in finite planar substrates using perfectly matched layers," IEEE Trans. Antennas Propag. **49**, 185–195 (2001).
28. R. W. Ziolkowski and M. Tanaka, "FDTD analysis of PBG waveguides, power splitters and switches," Opt. Quantum Electron. **31**, 843–855 (1999).
29. I. El-Kady, M. M. Sigalas, R. Biswas, and K. M. Ho, "Dielectric waveguide in two-dimensional photonic bandgap materials," J. Lightwave Technol. **17**, 2042–2049 (1999).
30. C. Seassal, Y. Désières, X. Letartre, P. Rojo-Romeo, P. Viktorovitch, and T. Benyattou, "Optical coupling between a two-dimensional photonic crystal-based microcavity and single-line defect waveguide on InP membranes," IEEE J. Quantum Electron. **38**, 811–815 (2002).
31. L. Knockaert and D. De Zutter, "Laguerre-svd reduced-order modelling," IEEE Trans. Microwave Theory Tech. **48**, 1469–1475 (2000).